water

Article

Residual Sediment Transport in the Fine-Grained Jiangsu Coast under Changing Climate: The Role of Wind-Driven Currents

Jinshan Pu [1,2], Yongping Chen [1,2], Min Su [2], Jinya Mei [2], Xinyi Yang [2], Zhibin Yu [2] and Peng Yao [1,2,3,*]

1 State Key Laboratory of Hydrology-Water Resources and Hydraulic Engineering, Hohai University, Nanjing 210098, China
2 College of Harbour, Coastal and Offshore Engineering, Hohai University, 1 Xikang Road, Nanjing 210098, China
3 State Key Laboratory of Coastal and Offshore Engineering, Dalian University of Technology, Dalian 116024, China
* Correspondence: p.yao@hhu.edu.cn

Abstract: Residual sediment transport, which is influenced by many factors including tide, wind, and waves, controls coastal morphological changes on different time scales. For fine-grained coasts where the wave effects are limited, it is still unclear to what extent the wind-driven current can impact the residual sediment transport. Taking the fine-grained Jiangsu Coast as an example, this study aimed to identify the contribution of wind on residual sediment transport over different time scales using a newly developed model. On a seasonal scale, wind-induced sediment transport shows strong seasonal characteristics, where the residual transport is more significant in the winter and summer. Nevertheless, the tide plays a dominant role in both residual current and sediment transport and the annual sediment budget over the coast. On the scale of tidal cycles, the extreme winds overwhelm the tides, controlling the residual sediment transport. However, the net sediment transport caused by the northerly winds (representing cold waves) is comparable to that of the southerly winds (representing typhoons). Therefore, although extreme winds can drive massive sediment transport in a short period, their contribution to annual sediment transport is limited.

Keywords: residual sediment transport; residual current; wind effect; tide; the Jiangsu Coast

check for updates

Citation: Pu, J.; Chen, Y.; Su, M.; Mei, J.; Yang, X.; Yu, Z.; Yao, P. Residual Sediment Transport in the Fine-Grained Jiangsu Coast under Changing Climate: The Role of Wind-Driven Currents. *Water* **2022**, *14*, 3113. https://doi.org/10.3390/w14193113

Academic Editor: Bommanna Krishnappan

Received: 29 August 2022
Accepted: 24 September 2022
Published: 2 October 2022

1. Introduction

Sediment transport is of great importance for the formation of turbidity maximum zone, substance transportation, and morphological evolution in estuaries, tidal flats, and offshore areas. Many studies have concentrated on sediment transport and morphological mechanisms over the last decades [1–5]. Sediment transport exhibits complicated patterns and processes under the effect of various factors, including tide, estuarine circulation, wind, waves and storms, sediment supplement, and erodibility, as well as humans [6–10]. These factors and physical processes act together or individually, remarkably impacting sediment transport on different temporal and spatial scales in coastal environments [11–13].

Residual sediment transport refers to the average sediment transport over a certain period, such as a tidal cycle, month, season, year, and other time scales, and which controls the medium- to long-term morphological change in coastal regions [14,15]. Tide is the primary force that drives sediment into suspension, leading to suspended sediment transport. When oceanic tides propagate into shallow coastal regions such as estuaries, tidal flats, and lagoons, the flooding tide differs from the ebb in terms of the tidal current velocity, duration time, etc., namely resulting in tidal asymmetry. Tidal asymmetry in estuaries and lagoons (tidal basins) is the main contributor to the residual current and sediment transport. For coarse-grained coasts, the sediment grains immediately respond to the tidal current so that the residual sediment transport is in line with the residual flow [16,17]. It is worth noting that for coarse-grained coasts (i.e., those with a sand-dominated bed), the sand supply from the rivers, which mainly moves in a bedload transport or bedform migration, is also a crucial factor in the sedimentary budget of a beach [18]. Fine-grained sediment transport is affected by settling and erosion lags between the sediment grain and tidal current, bringing more complexities in understanding residual sediment transport.

In addition to the tide, wind can also drive the suspended sediment transport and the residual sediment transport on different temporal and spatial scales, and its effect has received significant attention in the literature [19–28]. Carniello et al. [23] developed a numerical model which combines wind waves with tidal currents in a shallow tidal basin of Venice, Italy. They validated that the wind shear stress modified the tidal hydrodynamics by introducing residual circulations, and wind waves were responsible for sediment erosion and resuspension by affecting the bottom shear stresses. By considering both wave and tidal currents in the numerical model, the estimation of the bottom shear stress and description of the processes responsible for the morphological evolution were improved in shallow tidal environments [21]. On the other hand, some scholars have demonstrated the importance of wind-driven flows on sediment transportation and morphological evolution [26,29–32]. For example, in the Wadden Sea, the wind-induced fluxes can cause water and sediment exchange over the tidal divides, leading to an interconnected morphodynamic evolution of the adjacent tidal basin [31,33]. Colosimo et al. [34] revealed that the wind indeed plays a paramount role in tidal flat sediment dynamics, not only relating to the wave-induced resuspension but also to the generation of wind-driven flows that enhance the tide-induced advection of sediment, eventually affecting the net sediment transport and morphodynamics of the intertidal areas.

For coarse-grained sandy beds, the active wind-driven sediment transport only appeared under the condition of weak tidal currents with strong waves. In the coastal region, where the tidal currents are weak, the waves contribute to bringing sediment into suspension. The wind-driven current serves as an agent to transport the suspensions. For fine-grained coasts, where the wave effect is limited, the extent to which the wind-driven sediment transport will affect the sediment budget on different time scales remains unclear. Especially under the condition of global climate change, local wind climatology and extreme wind conditions may change. The Jiangsu Coast, located in eastern China (Figure 1), has a nearly 1000 km straight and fine-grained coastline. Yu [35] reported that extreme wind intensity has increased in recent decades due to climate change. Thus, the Jiangsu Coast is an ideal case to study the effects of wind on residual sediment transport. Understanding the contribution of wind to the residual suspended sediment transport on different scales can further integrate the knowledge of the coastal morphological change in the context of the changing climate.

In this study, a newly proposed, multi-fraction sediment transport model was employed to explain the net sediment transport process in the central Jiangsu Coast, China. We aimed to: (1) investigate the residual suspended sediment transport process under the influence of tide and wind; and (2) determine the contribution of tide and wind to the residual suspended sediment transport along the Jiangsu Coast. This paper is organized as follows. In Section 2, the general information of the study area, wind data, and modeling method are outlined. The results are provided in Section 3, including the Eulerian residual current and residual sediment transport patterns under different conditions. Discussions are contained in Section 4 with respect to the comparative importance of tide and wind on the sediment budget at different scales. The conclusions are in Section 5.

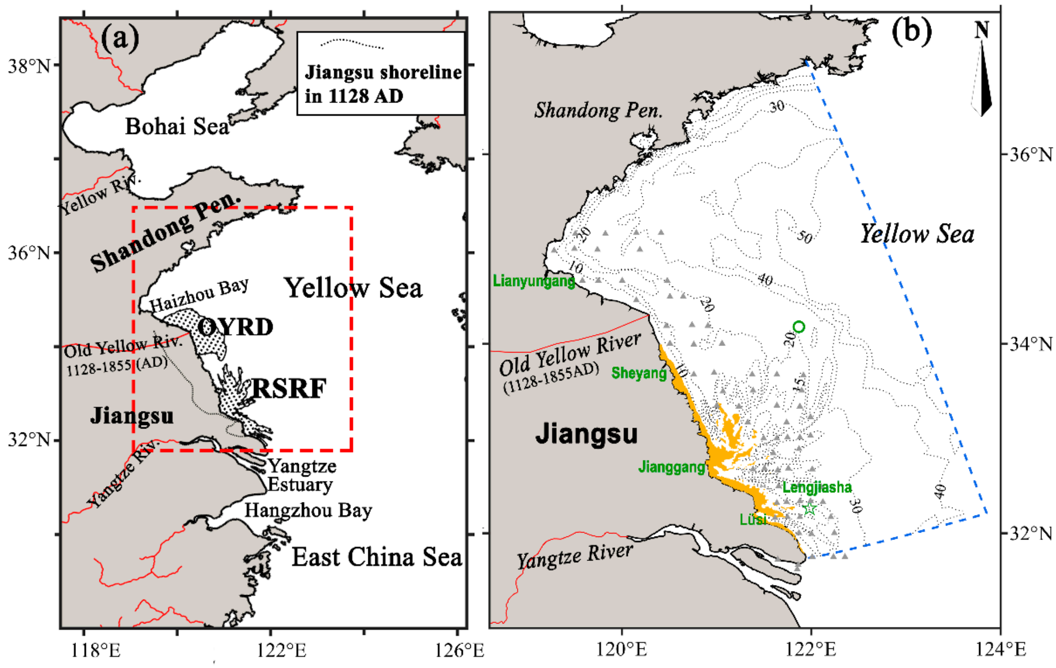

Figure 1. (**a**) Regional setting of the Jiangsu Coast with two featured geomorphic units: the Old Yellow River delta (OYRD) and the radial sand ridge field (RSRF). (**b**) The JRM model region (modified from Yao et al. [36]). In (**b**), the Lengjiasha buoy station is marked with a star symbol and the tidal flats are highlighted in yellow.

2. Materials Data and Methods

2.1. Study Area

The Jiangsu Coast, which faces the South Yellow Sea, is located in eastern China (Figure 1). The silty coast dominates ~93% of the total shoreline, which is attributed to two large silt-laden rivers: The Yellow River and Yangtze River. The Yellow River used to discharge into the South Yellow Sea via the north Jiangsu Coast during the period of 1128–1855 AD, forming not only the Old Yellow River delta (OYRD) but also a large area of tidal flats in the south. However, since 1855, the Yellow River transferred to the north, discharging into the Bohai Sea and resulting in a severe erosion in the OYRD (Figure 1a). The eroded silt-sized materials interact and merge with local deposits in different regions along the Jiangsu Coast, such as the fan-shaped radial sand ridge field (RSRF) in the south and has resulted in the diverse sedimentary environment observed nowadays. Generally, the particle size of the bottom sediment grains ranges from 8 to 250 μm, with pronounced silt contents.

The Jiangsu Coast is exposed to the subtropical monsoon climate. The wind is predominantly from the NE or N in the winter and from the SE or SSE in the summer. Statistically, the NE wind is stronger than the SE, and the average wind speed over the sea surface is between 5 and 7 m/s [37]. Detailed wind analyses are presented in Section 2.2. The waves are mainly controlled by monsoon climates and vary spatially and temporally, with significant wave heights smaller than 1 m. The tide, especially the semi-diurnal tide, is the dominant force in the Yellow Sea [38–40]. The mean tidal range along the coast is between 2 and 4 m. The mean tidal flow velocity is weak in the Haizhou Bay (between 0.3 and 0.5 m/s) and OYRD (between 0.6 and 1 m/s), and it becomes very strong in the RSRF. The mean tidal flow velocity can be larger than 2 m/s in several major tidal channels of the RSRF during the spring tide [39].

2.2. Wind Data

A previously established numerical model (the Jiangsu Regional Model, see Section 2.3) was utilized to explore the wind impact on the sediment transport of the Jiangsu Coast. It is necessary to have spatial varying wind data with enough of a temporal resolution to drive the numerical model [36]. However, considering the large spatial scale of the Jiangsu Coast, it is challenging to produce the spatial varying wind field data by individual wind stations. Therefore, global wind datasets derived from satellite and reanalysis were selected to generate the wind field. In this study, four global wind datasets were addressed: the National Centers for Environmental Prediction (NCEP) reanalysis dataset [41], Quick Scatterometer and NCEP blended wind (QSCAT) dataset [42], Cross-Calibrated Multi-Platform (CCMP) dataset [43], and European Centre for Medium-Range Weather Forecasts (ECMWF) Reanalysis v5 (ERA5) dataset [44]. We also collected one-year wind data (2008.10–2009.10) at an offshore buoy to validate these datasets (see Lengjiasha in Figure 1b). As the aforementioned wind datasets from both the satellite and reanalysis data are referred to at a height of 10 m, the buoy wind data had to be first converted to reflect the wind speed at 10 m above the mean sea level before comparison, following the procedure of Alvarez et al. [45].

Figure 2 shows the comparisons of wind speed between four datasets and the buoy wind data during the four seasons. In different seasons, the wind speed of all four datasets follows the variation trend of the buoy data. The differences between the different datasets are also minor. Table 1 lists the statistical metrics (i.e., root-mean-square deviations, bias, and standard deviations) between the datasets and the measurement. The CCMP provides the smallest RMS, bias, and STD, showing the best agreement with buoy data. The performance of ERA5 is not as perfect as the CCMP, but better than the other datasets. However, the time span of the data record for the CCMP is from 1989 to the present, while for the ERA5, it is from 1959 to the present. Considering both the accuracy and the period of the data record, the ERA5 dataset was selected to spatiotemporally generate the varying wind data for the numerical model.

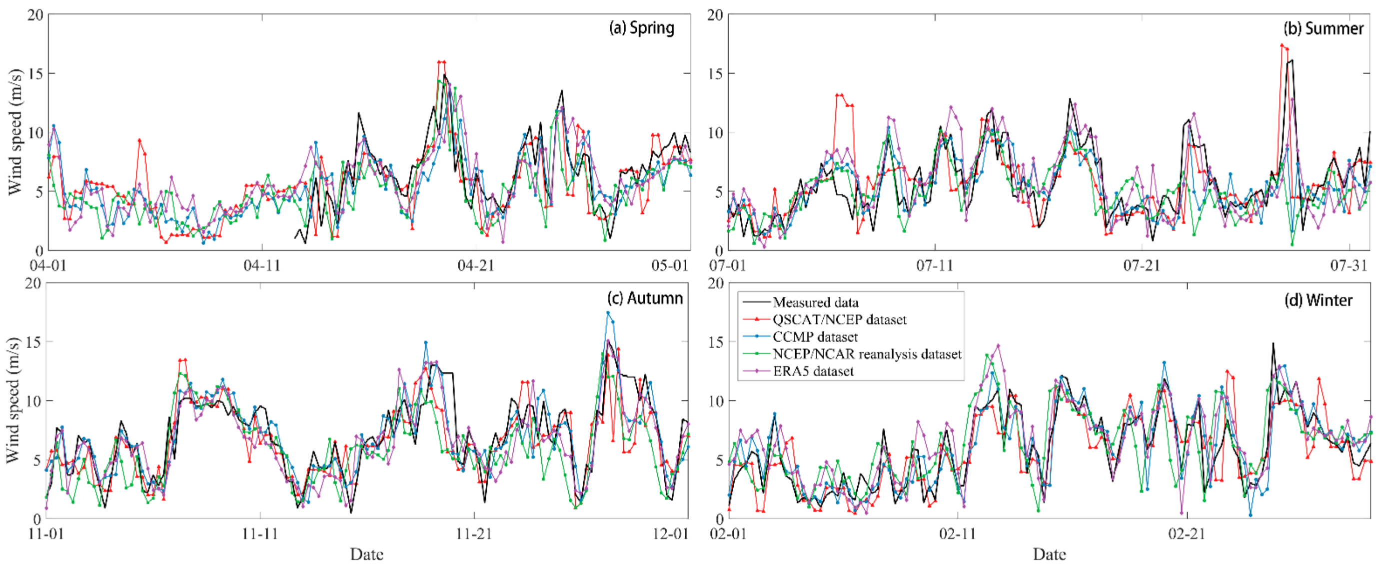

Figure 2. Comparison of the wind speed in four seasons between the Lengjiasha buoy data and global wind datasets.

Based on the ERA5 dataset, we extracted wind data from 1959 to the present at the central location of the study area (Figure 1a). The wind rose figure shows that the frequent wind direction is from the north (N) and the south-southeast (SSE) (Figure 3). The maximum annual wind speeds from these two directions were determined to analyze the impact of climate change (Figure 4). The intensity of the extreme northerly winds showed a slowly increased trend while the SSE direction remained nearly unchanged. The northerly wind is mainly affected by winter cold waves, and the southerly wind is affected by typhoons. Thus, the cold wave is relatively more sensitive to the changing climate in the study area.

Table 1. Comparison among the diverse global wind datasets.

Wind	NCEP			QSCAT		
	RMS	Bias	STD	RMS	Bias	STD
Speed	2.78	0.40	2.75	2.50	0.15	2.50
Direction	62.45	−8.03	61.93	61.62	−2.55	61.57
Wind	**CCMP**			**ERA5**		
	RMS	**Bias**	**STD**	**RMS**	**Bias**	**STD**
Speed	2.34	−0.13	2.34	2.39	−0.25	2.37
Direction	54.33	−1.00	54.32	55.77	−3.68	55.65

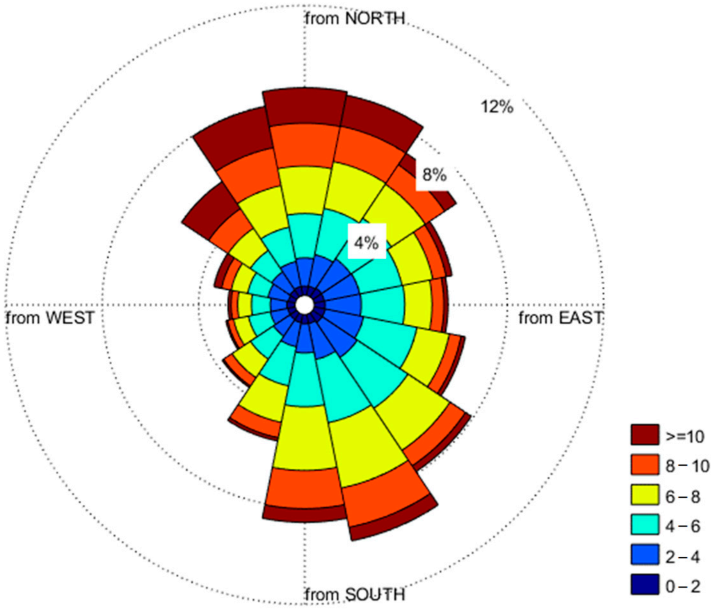

Figure 3. Wind rose map in the center of the study area, generated based on the ERA5 dataset from 1959 to 2019.

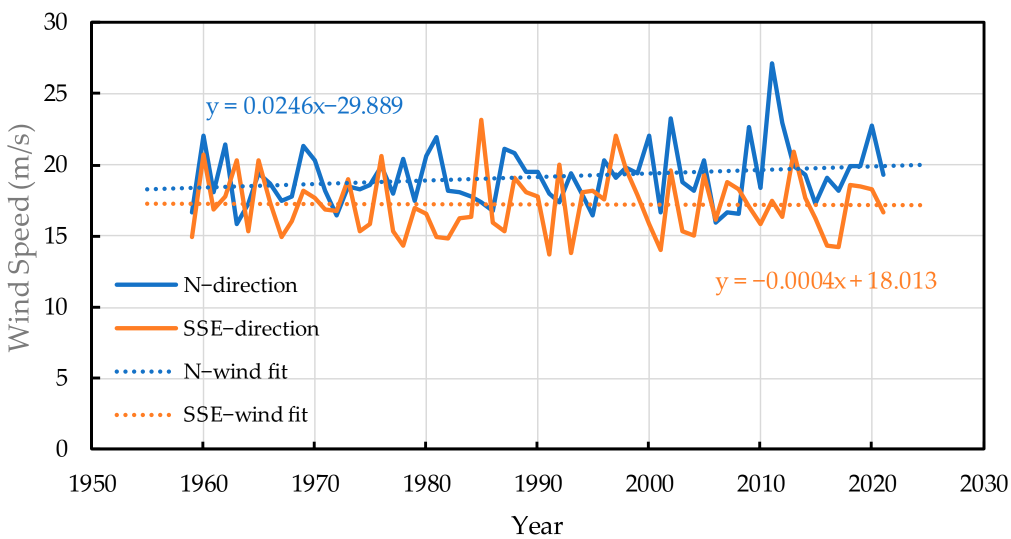

Figure 4. The variation of the annual maximum wind speed in the N and SSE directions, respectively.

2.3. Sediment Transport Modeling and Modeling Scenarios

The Jiangsu Regional Model (referred to as the JRM) was set up based on the open-source version of Delft3D. The JRM has been applied to model the sediment transport in the Jiangsu Coast with satisfactory accuracy from the time scales of days to years under tidal-only conditions [36]. This study utilized the JRM by considering the effect of wind on sediment transport using the ERA5 wind dataset.

The JRM, with a range of latitude between 32° and 36.5° and longitude between 119° and 124°, covers the entire inner shelf along the Jiangsu Coast (Figure 1b). The boundary-fitted orthogonal curvilinear grid with a size range from 0.42′ to 0.71′ (i.e., 608–1216 m) was selected under the spherical coordinates, and 13 tidal harmonic components (i.e., M2, S2, K2, N2, K1, O1, P1, Q1, M4, MS4, MN4, MF, and MM) were applied to drive the model along two open boundaries.

As mentioned before, the Jiangsu Coast features a fine-grained and silt-dominated sea bottom, but the sediment composition varies in different sub-regions. In the literature, the silt-enriched sediment mixtures have been reported to hold the dual features of both non-cohesive and cohesive sediments [46–49]. Therefore, a multi-fraction sediment transport model was used to calculate the sediment transport [48]. This module was derived from the updated formulations of van Rijn [50,51] and has been validated by various laboratory experiments [48]. According to the representative sediments in the different regions, four sediment fractions, i.e., fine silt (i.e., 16 μm), silt (i.e., 45 μm), very fine sand (i.e., 90 μm), and fine sand (i.e., 180 μm), have been selected. For example, fine silt (i.e., 16 μm) is abundant in the OYRD, while silt (i.e., 45 μm) is the dominant sediment fraction in the tidal flats of the RSRF. The ridges of the RSRF are mainly composed of sandy fractions (i.e., 90 and 180 μm). Meanwhile, the original distribution of the bed composition was re-constructed in terms of the percentage of the four representative sediment fractions. More details about the model configurations and operations can be found in Yao et al. [36].

In this study, by using the JRM and the ERA5 wind dataset, we have designed several modeling scenarios to explore the wind impact on the sediment transport on different scales. On the seasonal scale, the modeling time range was set from June 2008 to June 2009. One-year spatial and temporal varying wind data were used to drive the model together with the astronomical tides. As a reference, we also ran the model in the same time span without wind, namely the tidal-only case. Thus, the wind effects could be obtained by subtracting the results of the tide-only case from the wind combined with tide case. On the tidal scale, we designed another two scenarios with extreme wind conditions. Based on the wind data analyses in Section 2.2, two wind directions (i.e., N and SSE) were selected as the representative wind directions during extreme weather. Because the northerly wind indicated a slow increase trend in the past decades (Figure 4), the average annual maximum wind speed from the north direction over the past 20 years (1999–2019), i.e., 19.65 m/s, was used as the representative extreme wind speed for both directions. These two extreme winds were set as a spatial and temporal constant to drive the model. For the extreme wind scenarios, the model first ran with 14 tidal cycles without wind as a reference, covering the spring and neap tides. Then, it was run with the wind from the two directions, mimicking the condition of extreme winds meeting different astronomical tidal periods. A prepared restart file (hot start) was used to initiate all the cases.

2.4. Data Process

In each case, both the Eulerian residual current and the residual sediment transport patterns have been calculated at each computational grid by:

$$U_E = \frac{1}{T}\int_{t_0}^{t_0+T} u(t)dt, \quad (1)$$

$$S = \frac{1}{T}\int_{t_0}^{t_0+T} s(t)dt \quad (2)$$

where U_E is the Eulerian residual current, u is the velocity at each grid (m/s), S is the residual sediment transport, s is the suspended sediment transport rate at each grid ($m^3/s/m$), and T is the averaging period. On the seasonal scale, T was three months; on the tidal scale, T represented 14 tidal cycles (one tidal cycle of semi-diurnal tides is 725 min). In both the one-year and 14 tidal-cycle cases that we ran, the output time interval is 30 min.

The dominance index (DI) was introduced to assess the comparative importance of the tide and wind on the current flux and sediment transport:

$$DI = \frac{A_{tide} - A_{wind}}{A_{tide} + A_{wind}}, \quad (3)$$

where A denotes the magnitude of the current velocity or suspended sediment transport. $DI = 0$ means the equal contribution of wind and tide. $DI > 0$ means tidal-dominated, and $DI < 0$ means wind-dominated.

3. Results

3.1. Eulerian Residual Current Pattern

Figure 5 depicts the tidally-driven and wind-induced Eulerian residual current fields of four seasons based on the one-year run cases, respectively. The DI distribution, represented by the background contour map, describes the comparative importance of the tide and wind in the different regions. In the four seasons, the tide-induced residual currents show similar magnitude and directions. That is, the residual currents are strong (>10 cm/s) in the shallow regions (i.e., RSRF) but weak (<5 cm/s) in the deep regions. In the OYRD, the Eulerian residual currents flow southward along the shore. Over the RSRF, the flow pattern becomes complex due to the coexistence of both onshore and offshore directions. However, the wind effects vary with the seasons. In the winter, the wind-driven current flows southward in the deeper regions (water depth > 20 m) with strong wind impacts (i.e., $DI < 1$), while the wind-driven current turns northward in summer. In the spring and autumn, the wind-driven residual currents are not strong enough to be distinguished. Thus, under the relatively weak wind in the spring and autumn, the residual current pattern is determined by the tide on the whole Jiangsu Coast. The wind effects on the residual current show substantial seasonal variations, and winters appear to have the most significant wind impact on the residual current.

Figure 6 shows the tidally-driven and wind-induced Eulerian residual current fields over the tidal cycles during extreme wind conditions, respectively. Except for several tidal channels, the wind overrules the tide in both direction and magnitude, dominating the residual current in the entire coastal region under extreme wind conditions. The direction of residual currents is mainly in line with the wind direction but follows the coastline. Furthermore, compared with the southerly wind, the northerly wind has more influence on the shallow regions, such as the tidal flats and sand ridges. That is, the northerly wind which is caused by the cold wave process in the winter has a more significant impact on the residual current than the southerly wind in the summer.

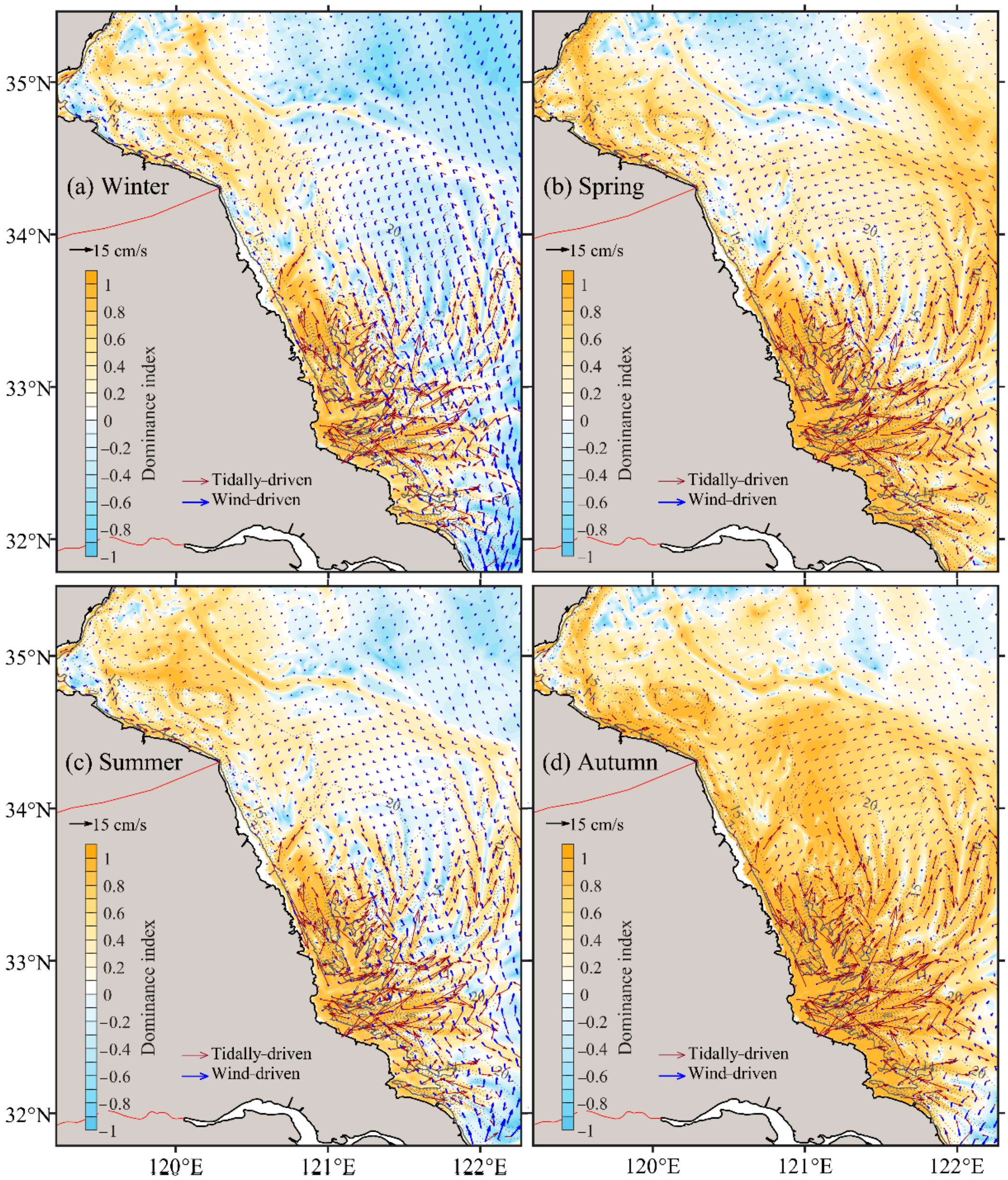

Figure 5. The tide- and wind-induced Eulerian residual currents in the four seasons: (**a**) winter, (**b**) spring, (**c**) summer, and (**d**) autumn. Note that the background map denotes the comparative importance of the wind and tide on the Eulerian residual currents.

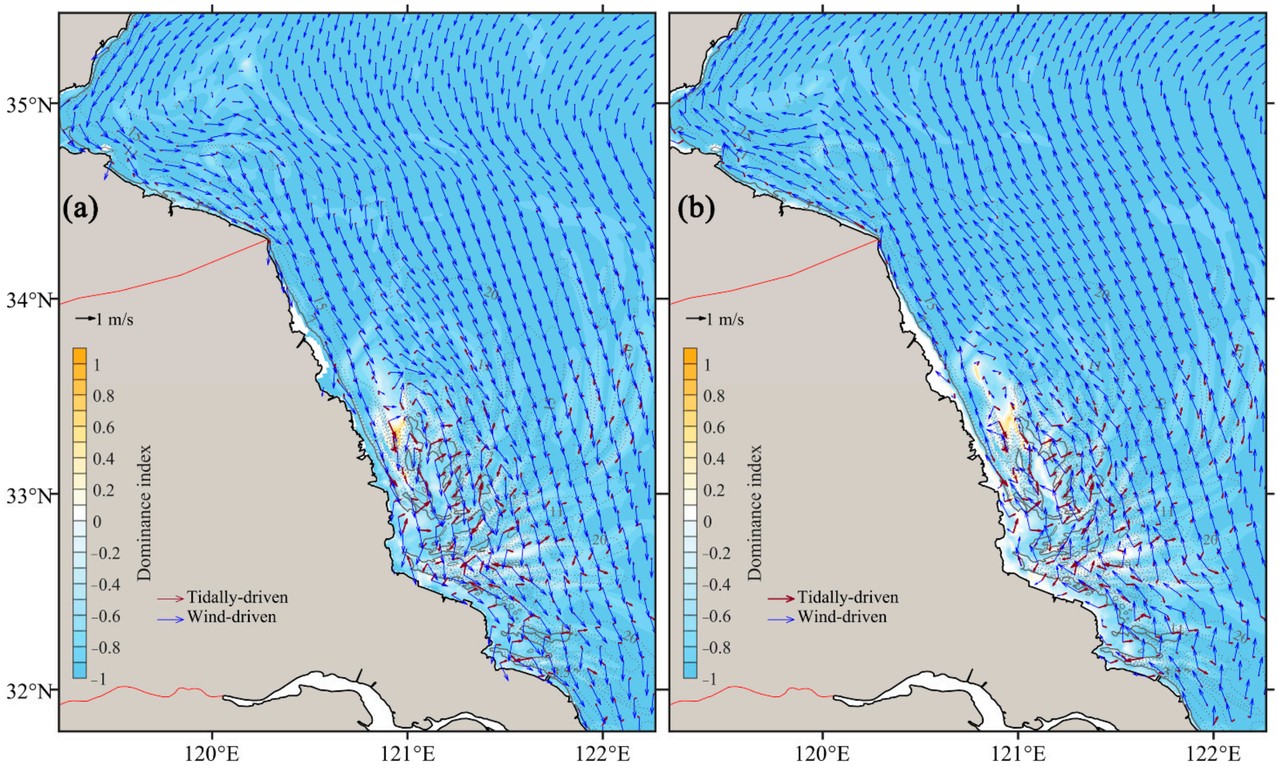

Figure 6. The tide- and wind-induced Eulerian residual currents in two extreme wind events: (**a**) N-direction wind, denoting the condition of a winter cold wave event; (**b**) SSE-direction wind, denoting a summer typhoon event. Note that the background map denotes the comparative importance of the wind and tide on the Eulerian residual currents.

3.2. Residual Sediment Transport Pattern

Figure 7 shows the tidally-driven and wind-induced residual sediment transport in the summer and winter seasons based on the one-year run cases, respectively. According to the residual current field (i.e., Figure 5), the results of spring and autumn are not displayed due to the weak wind effect. The results show that the residual sediment transport is only distinguishable in areas with a water depth smaller than 20 m. This differs from the Eulerian residual current pattern, as the suspended sediments are more active in shallow regions. In the north of the Jiangsu Coast, the tide-induced residual sediment transport occurs in a single direction: from the OYRD to the RSRF. In the south, onshore and offshore transport coexists under the tidal-only condition in both seasons. Similar to the Eulerian residual current pattern, the wind-induced sediment transport shows some features of seasonal change. In the summer, the wind-induced sediment transport is mainly directed northward, while it transfers to the opposite direction in the winter. The spatial variation of the *DI* suggests that the tidally-driven residual sediment transport dominates the large area of the Jiangsu Coastal waters on a seasonal scale. The wind influence on sediment transport only intensified and became comparable with the tide in the deep offshore regions.

Figure 8 depicts the tidally-driven and wind-induced residual sediment transport over the tidal cycles during extreme wind conditions, respectively. Similar to the residual transport over one year, the sediment transport is mainly in the areas with a water depth smaller than 20 m. However, the residual sediment transport outside of the RSRF is dominated by the wind-drive flow, and the transport direction is consistent with the wind direction. As shown by the *DI* map, the tidally-driven residual sediment transport is active only in the tidal flats, sand ridges, and deep tidal channels in the summer, while in the winter, the regions dominated by the tide are further squeezed to the tidal channels. This further indicates that the influence of the extreme north winds (representing cold waves) on sediment transport is stronger than that of extreme south winds (representing typhoons).

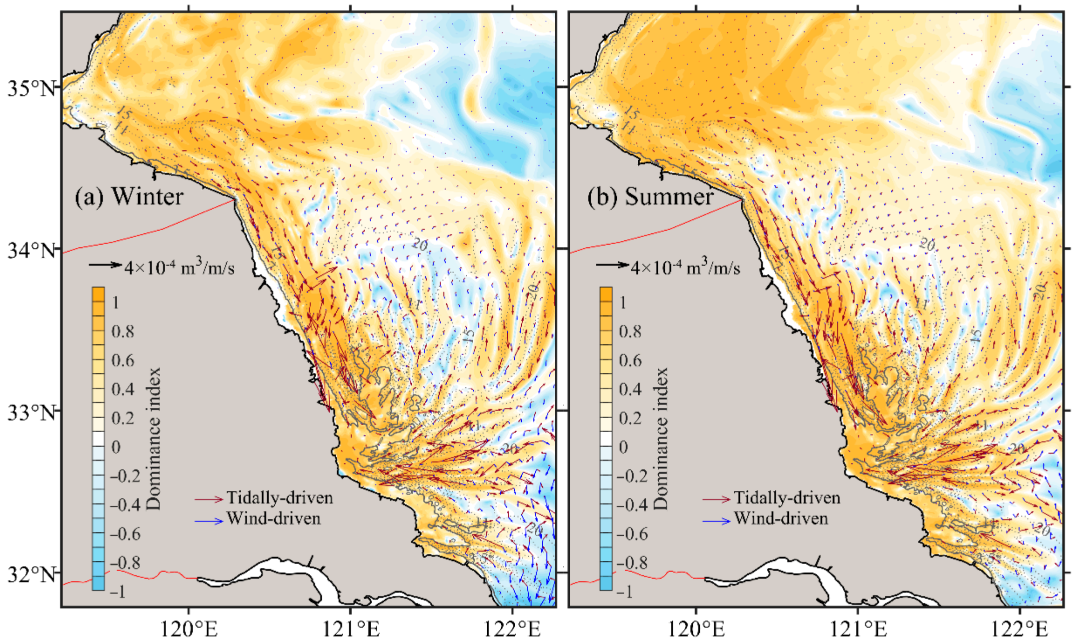

Figure 7. The tide- and wind-induced residual sediment transport in (**a**) winter and (**b**) summer, respectively. Note that the background map denotes the comparative importance of the tide- and wind-induced sediment transport.

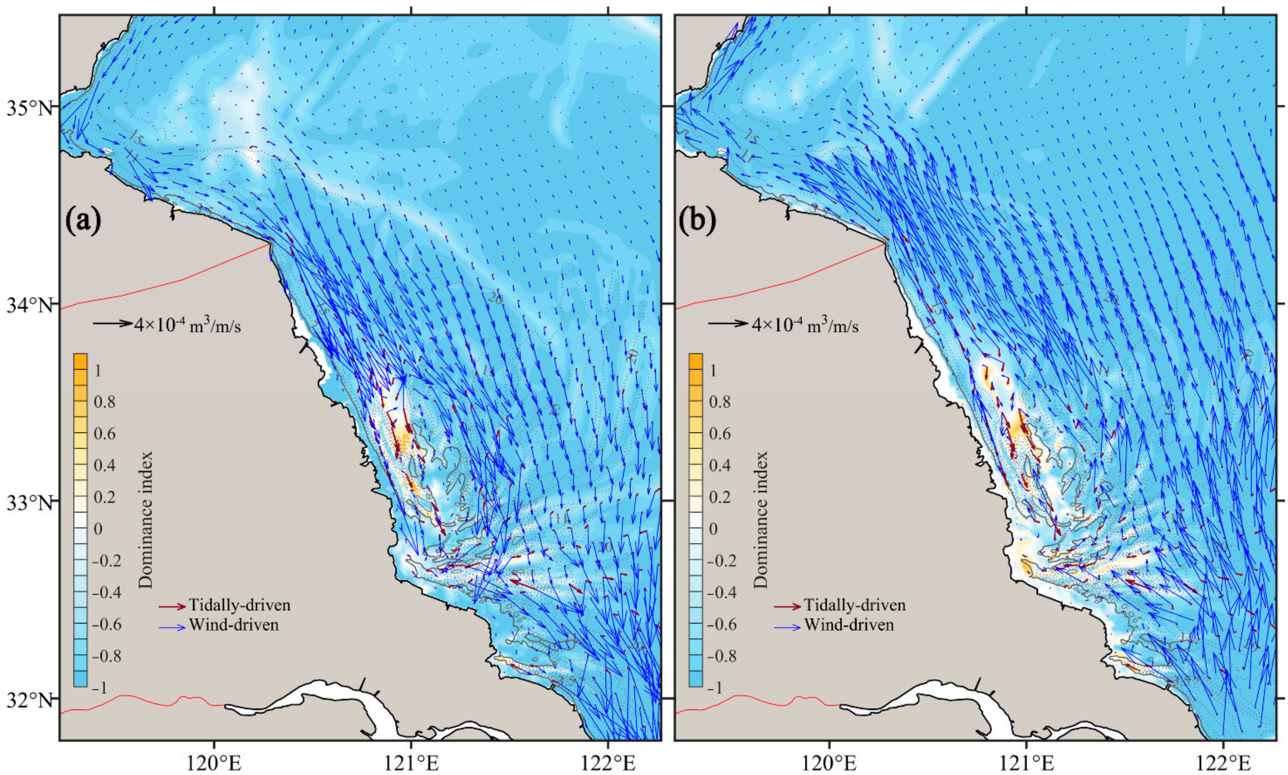

Figure 8. The tide- and wind-induced residual sediment transport in two extreme wind events: (**a**) N-direction wind, denoting the condition of a winter cold wave event; (**b**) SSE-direction wind, denoting a summer typhoon event. Note that the background map denotes the comparative importance of the tide- and wind-induced sediment transport.

4. Discussion

4.1. Wind Contribution to Residual Current and Sediment Transport in Different Regions

The numerical simulations have shown that the wind contribution varies on different spatial and temporal scales in both the Eulerian residual current and residual sediment transport. In order to quantitatively understand the wind contribution to the water and sediment transport, we statistically analyzed the temporal and spatial changes of the *DI* factor based on different numerical cases. The overall domain (i.e., the Jiangsu Coast) has been divided into four sub-regions based on the water depth (i.e., tidal flats region, <3.5 m; shallow region, 3.5–10 m; transition region, 10–20 m; deep waters, >20 m). In each numerical case, the *DI* in different sub-regions has been averaged so that the wind contribution on different time scales can be identified in different regions.

Regarding the seasonal time scale, the averaged *DI* of the residual currents in the four sub-regions with different water depths is shown in Figure 9a. Generally, the wind effect on the residual current progressively escalates as the water depth increases. The wind contribution to the residual current is the greatest in winter, followed by summer, spring, and autumn. The averaged *DI* of the residual sediment transport in regions with different water depths is shown in Figure 10a. Similar to the seasonal variations of the residual current, the wind-induced residual sediment transport is the strongest in the winter. However, in winter, wind shows dominating power on the residual current in water depths larger than 20 m; however, it has minimal impact on the residual sediment transport. The tide dominates the residual sediment transport in each season and region. This is because the suspended sediment concentration is higher nearshore and decreases seaward. Thus, the sediment transport in the deeper region is limited.

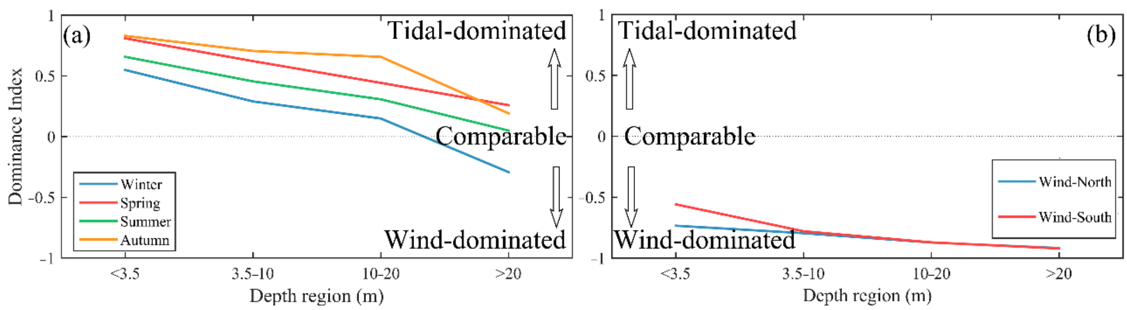

Figure 9. Comparative importance of the tide- and wind-induced Eulerian residual currents in different depth regions over the time scales of (**a**) seasonal and (**b**) tidal cycles.

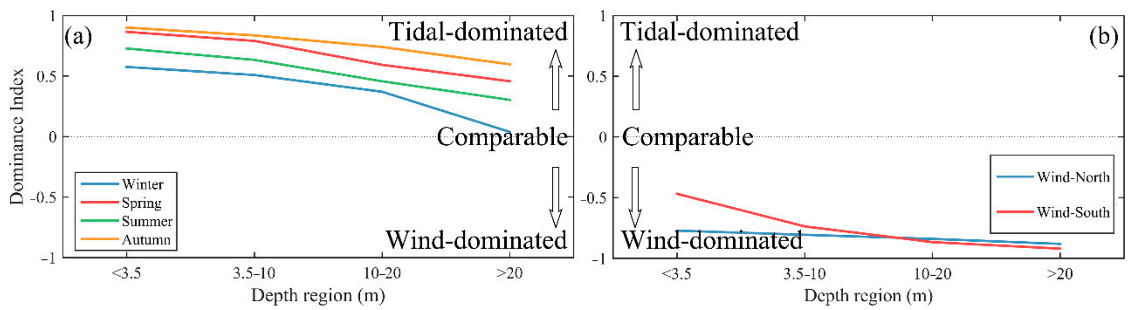

Figure 10. Comparative importance of the tide- and wind-induced residual sediment transport in different depth regions over the time scales of (**a**) seasonal and (**b**) tidal cycles.

Regarding the time scale of the tidal cycles, under extreme wind conditions, both the residual current and residual sediment transport are dominated by the wind (Figures 9b and 10b). The extreme southerly wind depicts a relatively weaker impact on the residual transport of water and sediment in the tidal flats (water depth < 3.5) compared with the northerly wind. For the regions with water depths greater than 10 m, the southerly wind shows an effect comparable to that of the northerly wind on both the residual current and sediment transport.

In summary, wind plays a substantial role only in extreme events over tidal scales. In contrast, on a seasonal scale, the tide is the dominant force that controls the residual sediment transport.

4.2. Wind Contribution to Sediment Budget along the Jiangsu Coast on Different Time Scales

To estimate the sediment budget along the Jiangsu Coast, we defined several large-scale littoral sectors similarly to our previous study [36]. Sector I, II, III, and IV represent the Haizhou Bay, OYRD, Sheyang Estuary, and RSRF, respectively (Figure 11). For the net sediment transport over an annual scale, both the tide-induced and wind-driven sediment budgets (the net sediment volume changes and transport pathways) within these sectors were calculated and are listed in Figure 11a and Table 2. Compared with the wind-driven sediment budget, the tide-induced sediment budget is much greater (Figure 11a), revealing the overwhelming effect of the tide on the net sediment transports over an annual scale. Furthermore, a significant characteristic we found was that the sediments that eroded from the OYRD are transported towards the RSRF, making the OYRD a vital sediment source for the RSRF in present conditions [52,53]. The wind-driven sediment transport directions are opposite to the tidal-only case that appeared in the boundaries, while the tidal-induced sediment transport pattern can hardly be changed.

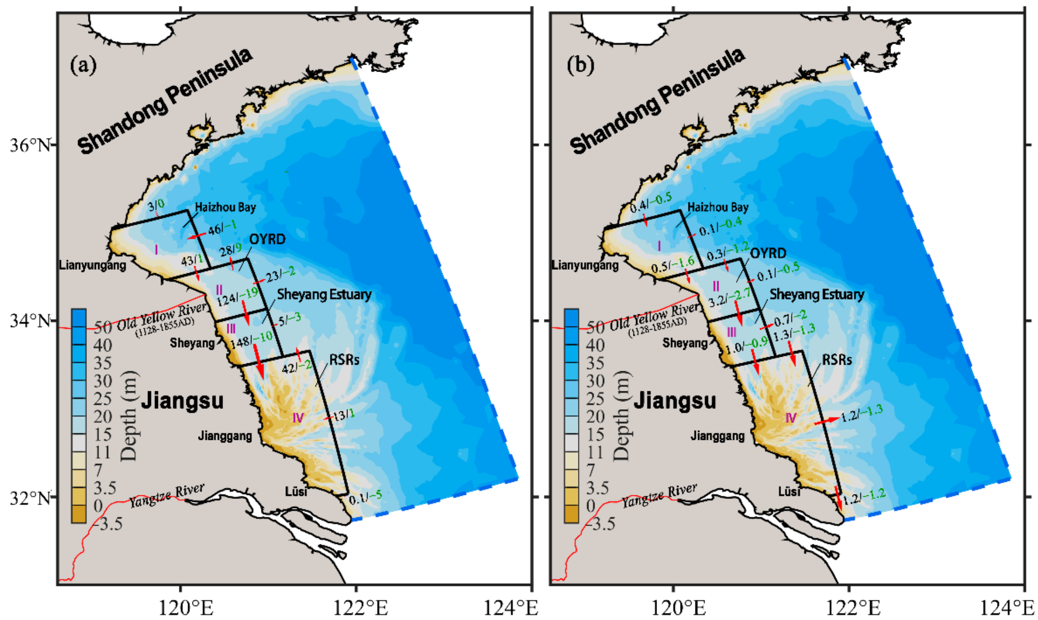

Figure 11. The tide- and wind-induced sediment budget in different sectors (**a**) over the annual scale and (**b**) over the tidal scale with extreme winds. In (**a**), the red arrows depict the sediment transport direction of the tide-only case and the black numbers depict the tide-induced sediment budget. The green numbers denote the wind-induced sediment budget, and a negative value means the opposite direction with the tide-only case. In (**b**), the red arrows and black numbers represent the wind-driven sediment transport under the extreme northerly wind, while the green numbers denote the wind-driven sediment transport under the extreme southerly wind; the negative value means an opposite direction to the northerly wind. Presented in Mm^3/year.

Table 2. The tide- and wind-induced sediment volume changes within each Sector, presented in Mm^3/year. Positive volumes mean sedimentation, while negative values denote erosion.

Sectors	I	II	III	IV
Tide-induced volume changes	6	−132	−29	124
Wind-induced volume changes	−2	13	−6	−12

For the net sediment volume changes within each Sector, the OYRD is under erosion (−132 Mm^3/year) while the RSRF's sediment volume increases at a rate of 124 Mm^3/year. The erosion amount in the OYRD is comparable to that of the sedimentation in the RSRF, suggesting that the erosion of the OYRD is the major contributor to the accretion of the RSRF. The wind effect can bring about 13 Mm^3 sedimentations in the OYRD and 12 Mm^3 erosion in the RSRF. Thus, the wind force generates an opposite pattern of erosion and sediment in the OYRD and RSRF, respectively, but the corresponding magnitude is limited compared with the tidal force.

Regarding the net sediment transport over the time scale of the tidal cycles, we have only calculated the wind-driven sediment budgets in different extreme conditions, and they are shown in Figure 11b; this is because the tidal-driven sediment budget is relatively small during the tidal cycles (i.e., 5–10 times smaller than the wind-driven net sediment transport). The magnitude of the sediment flux in each sub-region that is caused by the extreme southward and northward wind speed is the same, but in opposite directions, especially in the Sheyang Estuary and RSRF. In the north of the OYRD, the southerly wind can transport more sediment to the north than the northerly wind. This is because the suspended sediment concentration in the OYRD is much larger than that of the Haizhou Bay [36]. Thus, the southerly wind can transport more suspended sediment from the OYRD toward the north. On the one hand, the coastal area of Jiangsu suffers from both typhoons in the summer and cold wave events in the winter every year, which can result in the re-distribution of sediments in different areas. On the other hand, the typhoons drive the net transport of sediment to the north, while the cold waves bring the sediment back to the south. That is, although a large amount of transportation can be caused in a short period by extreme wind events, the northward transport can be balanced by the southward transport in most regions. This explains why the wind contribution is weak on the residual sediment transport over a seasonal scale (i.e., in Figure 10a).

4.3. Limitations and Remarks

This study carried out a numerical modeling study focusing on residual sediment transport over the seasonal and tidal time scales, respectively. The schematization methods placed on the representative wind were applied to different scenarios. For the one-year runs, the spatial and temporal varying wind field was selected based on the validated global wind dataset. For the runs of the tidal cycles, the schematized extreme wind with a constant direction and intensity was chosen, favorable for understanding the re-distribution of the suspended sediment under extreme conditions on an open coast. However, cold waves and typhoons have moving paths, generating spatial varying wind fields. Thus, it is necessary in the future to explore the suspended sediment dynamics while considering spatial and temporal varying wind fields in detail during extreme. In addition, wind can generate waves, which are further responsible for sediment suspension in shallow regions. Although previous studies have proposed that waves play a secondary role in the residual sediment transport along the Jiangsu Coast [54,55], it is still essential to understand the wave contribution at different scales and to shed light on coastal morphodynamics under changing climate. This is also a critical issue that needs to be studied in the future.

5. Conclusions

Applying a newly developed JRM model, this study has investigated the contribution of wind to the residual sediment transport patterns in the fine-grained Jiangsu Coast. By comparing global wind datasets with buoy wind data, the ERA5 wind dataset was selected to generate the wind field and to drive the model on different scales. The conclusions are listed as follows:

(1) Over the seasonal time scale, the wind-induced residual transport of water and sediment shows strong seasonal variations. In the winter, the wind-driven residual sediment transport direction is to the south, while it changes to the north in the summer. However, in the spring and autumn, the low-intensity wind can hardly affect the transport of sediments. The tide plays a substantial role in residual sediment transport in both shallow (water depth < 10 m) and deep regions (water depth > 20 m). The annual sediment budget also indicates the predominant influence of tide on the sediment transport patterns and morphological changes of the Jiangsu Coast. In contrast, the influence of wind on the morphological evolution of the Jiangsu Coast is not remarkable over an annual scale.

(2) Over the tidal cycle time scale, the wind during extreme events (i.e., cold waves in the winter or typhoons in the summer) controls both the residual current and sediment transport. Regarding tidal flats and shallow shoals, the extreme northerly wind is more effective than the southerly wind. However, the net sediment transport over the tidal cycle caused by the northerly winds is comparable to that of the southerly winds on the open coastline.

Author Contributions: Conceptualization, P.Y. and Y.C.; methodology, P.Y.; software, J.P. and J.M.; validation, M.S. and J.P.; formal analysis, J.P. and Z.Y.; data curation, P.Y.; writing—original draft preparation, J.P. and P.Y.; writing—review and editing, M.S. and Y.C.; visualization, X.Y. and J.P.; funding acquisition, J.P., Y.C., Z.Y. and P.Y. All authors have read and agreed to the published version of the manuscript.

Funding: This research was funded by the Fundamental Research Funds for the Central Universities of China (Grant No. B200204017, 2018B637X14, and 2019B05914), National Natural Science Foundation of China (Grant No. 51979076, 51620105005, and 51809296), Postgraduate Research & Practice Innovation Program of Jiangsu Province (Grant No. KYCX18_0605), and Open Foundation of State Key Laboratory of Coastal and Offshore Engineering (Dalian University of Technology) (Grant No. LP2207).

Data Availability Statement: Wind datasets used in this study were obtained from National Oceanic and Atmospheric Administration (NOAA), National Centers for Environmental Prediction (NCEP), National Center for Atmospheric Research (NCAR), and European Centre for Medium-Range Weather Forecasts (ECMWF) and are freely available at https://psl.noaa.gov, www.remss.com/measurements/ccmp, and https://www.ecmwf.int/.

Conflicts of Interest: The authors declare no conflict of interest.

References

1. Burchard, H.; Schuttelaars, H.M.; Ralston, D.K. Sediment Trapping in Estuaries. *Annu. Rev. Mar. Sci.* **2018**, *10*, 371–395. [CrossRef] [PubMed]
2. Elias, E.P.L.; Hansen, J.E. Understanding processes controlling sediment transports at the mouth of a highly energetic inlet system (San Francisco Bay, CA). *Mar. Geol.* **2013**, *345*, 207–220. [CrossRef]
3. Gatto, V.M.; Van Prooijen, C.B.; Wang, Z.B. Net sediment transport in tidal basins: Quantifying the tidal barotropic mechanisms in a unified framework. *Ocean Dyn.* **2017**, *67*, 1385–1406. [CrossRef]
4. Li, Z.; Jia, J.; Wang, Y.P.; Zhang, G. Net suspended sediment transport modulated by multiple flood-ebb asymmetries in the progressive tidal wave dominated and partially stratified Changjiang Estuary. *Mar. Geol.* **2022**, *443*, 106702. [CrossRef]
5. Ralston, D.K.; Geyer, W.R. Episodic and Long-Term Sediment Transport Capacity in The Hudson River Estuary. *Estuaries Coasts* **2009**, *32*, 1130–1151. [CrossRef]
6. Brouwer, R.L.; Schramkowski, G.P.; Dijkstra, Y.M.; Schuttelaars, H.M. Time Evolution of Estuarine Turbidity Maxima in Well-Mixed, Tidally Dominated Estuaries: The Role of Availability- and Erosion-Limited Conditions. *J. Phys. Oceanogr.* **2018**, *48*, 1629–1650. [CrossRef]
7. Chernetsky, A.S.; Schuttelaars, H.M.; Talke, S.A. The effect of tidal asymmetry and temporal settling lag on sediment trapping in tidal estuaries. *Ocean Dyn.* **2010**, *60*, 1219–1241. [CrossRef]
8. Dijkstra, Y.M.; Schuttelaars, H.M.; Schramkowski, G.P.; Brouwer, R.L. Modeling the Transition to High Sediment Concentrations as a Response to Channel Deepening in the Ems River Estuary. *J. Geophys. Res. Oceans* **2019**, *124*, 1578–1594. [CrossRef]

9. Wei, X.; Kumar, M.; Schuttelaars, H.M. Three-Dimensional Sediment Dynamics in Well-Mixed Estuaries: Importance of the Internally Generated Overtide, Spatial Settling Lag, and Gravitational Circulation: Sediment dynamics in well-mixed estuary. *J. Geophys. Res. Oceans* **2018**, *123*, 1062–1090. [CrossRef]
10. Zhang, G.; Chen, Y.; Cheng, W.; Zhang, H.; Gong, W. Wave Effects on Sediment Transport and Entrapment in a Channel-Shoal Estuary: The Pearl River Estuary in the Dry Winter Season. *J. Geophys. Res. Oceans* **2021**, *126*, e2020JC016905. [CrossRef]
11. Chen, L.; Gong, W.; Scully, M.E.; Zhang, H.; Cheng, W.; Li, W. Axial Wind Effects on Stratification and Longitudinal Sediment Transport in a Convergent Estuary During Wet Season. *J. Geophys. Res. Oceans* **2020**, *125*, e2019JC015254. [CrossRef]
12. Gong, W.; Jia, L.; Shen, J.; Liu, T.J. Sediment transport in response to changes in river discharge and tidal mixing in a funnel-shaped micro-tidal estuary. *Cont. Shelf Res.* **2014**, *76*, 89–107. [CrossRef]
13. Sommerfield, C.K.; Wong, K.C. Mechanisms of sediment flux and turbidity maintenance in the Delaware Estuary. *J. Geophys. Res. Oceans* **2011**, *116*, C01005. [CrossRef]
14. Guo, L.; Brand, M.; Sanders, B.F.; Foufoula-Georgiou, E.; Stein, E.D. Tidal asymmetry and residual sediment transport in a short tidal basin under sea level rise. *Adv. Water Resour.* **2018**, *121*, 1–8. [CrossRef]
15. Bolle, A.; Wang, Z.B.; Amos, C.; Ronde, J. The influence of changes in tidal asymmetry on residual sediment transport in the Western Scheldt. *Cont. Shelf Res.* **2010**, *30*, 871–882. [CrossRef]
16. Van Maren, D.S.; Gerritsen, H. Residual flow and tidal asymmetry in the Singapore Strait, with implications for resuspension and residual transport of sediment. *J. Geophys. Res. Oceans* **2011**, *117*, C04021. [CrossRef]
17. Chu, A.; Wang, Z.; de Vriend, H.J. Analysis on residual coarse sediment transport in estuaries. *Estuar. Coast. Shelf Sci.* **2015**, *163*, 194–205. [CrossRef]
18. Cilli, S.; Billi, P.; Schippa, L.; Grottoli, E.; Ciavola, P. Bedload transport and dune bedforms characteristics in sand-bed rivers supplying a retreating beach of the northern Adriatic Sea (Italy). *J. Hydrol. Reg. Stud.* **2021**, *37*, 100894. [CrossRef]
19. Bassoullet, P. Sediment transport over an intertidal mudflat: Field investigations and estimation of #uxes within the 'Baie de Marennes-Olerona (France). *Cont. Shelf Res.* **2000**, *20*, 1635–1653.
20. Blaas, M.; Kerkhoven, D.; de Swart, H. Large-scale circulation and flushing characteristics of the North Sea under various climate forcings. *Clim. Res.* **2001**, *18*, 47–54. [CrossRef]
21. Carniello, L.; D'Alpaos, A.; Definaa, A. Modeling wind waves and tidal flows in shallow micro-tidal basins. *Estuar. Coast. Shelf Sci.* **2011**, *92*, 263–276. [CrossRef]
22. Carniello, L.; Defina, A.; D'Alpaos, L. Morphological evolution of the Venice lagoon: Evidence from the past and trend for the future. *J. Geophys. Res. Earth Surf.* **2009**, *114*, F04002. [CrossRef]
23. Carniello, L.; Defina, A.; Fagherazzi, S.; D'Alpaos, L. A combined wind wave-tidal model for the Venice lagoon, Italy: A combined wind wave-tidal model. *J. Geophys. Res. Earth Surf.* **2005**, *110*, F04007. [CrossRef]
24. Friedrichs, C.T. *Tidal Flat Morphodynamics: A Synthesis*; William & Mary: Williamsburg, VA, USA, 2011.
25. Green, M.O.; Coco, G. Review of wave-driven sediment resuspension and transport in estuaries. *Rev. Geophys.* **2014**, *52*, 77–117. [CrossRef]
26. Mariotti, G.; Fagherazzi, S. Wind waves on a mudflat: The influence of fetch and depth on bed shear stresses. *Cont. Shelf Res.* **2013**, *60*, S99–S110. [CrossRef]
27. Smith, J.A.; Damm, P.E.; Skogen, M.D.; Flather, R.A.; PÄtsch, J. An investigation into the variability of circulation and transport on the north-west european shelf using three hydrodynamic models. *Dtsch. Hydrogr. Z.* **1996**, *48*, 325–348. [CrossRef]
28. Zhu, Q.; van Prooijen, B.C.; Wang, Z.B.; Yang, S.L. Bed-level changes on intertidal wetland in response to waves and tides: A case study from the Yangtze River Delta. *Mar. Geol.* **2017**, *385*, 160–172. [CrossRef]
29. Baeye, M.; Fettweis, M.; Voulgaris, G.; Van Lancker, V. Sediment mobility in response to tidal and wind-driven flows along the Belgian inner shelf, southern North Sea. *Ocean Dyn.* **2011**, *61*, 611–622. [CrossRef]
30. Christiansen, C.; Vølund, G.; Lund-Hansen, L.C.; Bartholdy, J. Wind influence on tidal flat sediment dynamics: Field investigations in the Ho Bugt, Danish Wadden Sea. *Mar. Geol.* **2006**, *235*, 75–86. [CrossRef]
31. Duran-Matute, M.; Gerkema, T.; de Boer, G.; Nauw, J.; Gräwe, U. Residual circulation and fresh-water transport in the Dutch Wadden Sea: A numerical modeling study. *Ocean Sci. Discuss* **2013**, *11*, 197–257. [CrossRef]
32. Talke, S.A.; Stacey, M.T. Suspended sediment fluxes at an intertidal flat: The shifting influence of wave, wind, tidal, and freshwater forcing. *Cont. Shelf Res.* **2008**, *28*, 710–725. [CrossRef]
33. Sassi, M.; Duran-Matute, M.; van Kessel, T.; Gerkema, T. Variability of residual fluxes of suspended sediment in a multiple tidal-inlet system: The Dutch Wadden Sea. *Ocean Dyn.* **2015**, *65*, 1321–1333. [CrossRef]
34. Colosimo, I.; de Vet, P.L.M.; van Maren, D.S.; Reniers, A.J.H.M.; Winterwerp, J.C.; van Prooijen, B.C. The Impact of Wind on Flow and Sediment Transport over Intertidal Flats. *J. Mar. Sci. Eng.* **2020**, *8*, 910. [CrossRef]
35. Yu, H. *The Impacts of Wind Fields on Sea Level at Jiangsu Offshore under the Climate Warming Conditions*; Nanjing University of Information Science and Technology: Nanjing, China, 2014.
36. Yao, P.; Su, M.; Wang, Z.; van Rijn, L.C.; Zhang, C.; Stive, M.J.F. Modelling tidal-induced sediment transport in a sand-silt mixed environment from days to years: Application to the Jiangsu coastal water, China. *Coast. Eng.* **2018**, *141*, 86–106. [CrossRef]
37. Zhang, C.K. *The Comprehensive Survey and Evaluation Report on Coastal Zone of Jiangsu Province*; Science Press: Beijing, China, 2012.
38. Choi, B.H. A Three-Dimensional Model of the East China Sea. In *Elsevier Oceanography Series*; Ichiye, T., Ed.; Ocean Hydrodynamics of the Japan and East China Seas; Elsevier: Amsterdam, The Netherlands, 1984; Volume 39, pp. 209–224.

39. Su, M.; Yao, P.; Wang, Z.B.; Zhang, C.K.; Stive, M.J.F. Tidal Wave Propagation in the Yellow Sea. *Coast. Eng. J.* **2015**, *57*, 1550008-1–1550008-29. [CrossRef]
40. Guohong, F. Tide and tidal current charts for the marginal seas adjacent to China. *Chin. J. Oceanol. Limnol.* **1986**, *4*, 1–16. [CrossRef]
41. Kalnay, E.; Kanamitsu, M.; Kistler, R.; Collins, W.; Deaven, D.; Gandin, L.; Iredell, M.; Saha, S.; White, G.; Woollen, J.; et al. The NCEP/NCAR 40-Year Reanalysis Project. *Bull. Am. Meteorol. Soc.* **1996**, *77*, 437–472. [CrossRef]
42. Hoffman, R.N.; Leidner, S.M. An Introduction to the Near–Real–Time QuikSCAT Data. *Weather Forecast.* **2005**, *20*, 476–493. [CrossRef]
43. Atlas, R.; Hoffman, R.N.; Ardizzone, J.; Leidner, S.M.; Jusem, J.C.; Smith, D.K.; Gombos, D. A Cross-calibrated, Multiplatform Ocean Surface Wind Velocity Product for Meteorological and Oceanographic Applications. *Bull. Am. Meteorol. Soc.* **2011**, *92*, 157–174. [CrossRef]
44. Hersbach, H.; Bell, B.; Berrisford, P.; Hirahara, S.; Horányi, A.; Muñoz-Sabater, J.; Nicolas, J.; Peubey, C.; Radu, R.; Schepers, D.; et al. The ERA5 global reanalysis. *Q. J. R. Meteorol. Soc.* **2020**, *146*, 1999–2049. [CrossRef]
45. Alvarez, I.; Gomez-Gesteira, M.; deCastro, M.; Carvalho, D. Comparison of different wind products and buoy wind data with seasonality and interannual climate variability in the southern Bay of Biscay (2000–2009). *Deep. Sea Res. Part II Top. Stud. Oceanogr.* **2014**, *106*, 38–48. [CrossRef]
46. Lamb, M.P.; Parsons, J.D. High-Density Suspensions Formed Under Waves. *J. Sediment. Res.* **2005**, *75*, 386–397. [CrossRef]
47. Te Slaa, S.; He, Q.; van Maren, D.S.; Winterwerp, J.C. Sedimentation processes in silt-rich sediment systems. *Ocean Dyn.* **2013**, *63*, 399–421. [CrossRef]
48. Yao, P.; Su, M.; Wang, Z.; van Rijn, L.C.; Zhang, C.; Chen, Y.; Stive, M.J.F. Experiment inspired numerical modeling of sediment concentration over sand–silt mixtures. *Coast. Eng.* **2015**, *105*, 75–89. [CrossRef]
49. Zuo, L.; Roelvink, D.; Lu, Y.; Wang, H. Modelling and analysis on high sediment concentration layer of fine sediments under wave-dominated conditions. *Coast. Eng.* **2018**, *140*, 205–231. [CrossRef]
50. Van Rijn, L.C. Unified View of Sediment Transport by Currents and Waves. I: Initiation of Motion, Bed Roughness, and Bed-Load Transport. *J. Hydraul. Eng.* **2007**, *133*, 649–667. [CrossRef]
51. Van Rijn, L.C. Unified View of Sediment Transport by Currents and Waves. II: Suspended Transport. *J. Hydraul. Eng.* **2007**, *133*, 668–689. [CrossRef]
52. Komar, P. The budget of littoral sediments, concepts and applications. *Shore Beach* **1996**, *64*, 18–26.
53. Su, M.; Yao, P.; Wang, Z.B.; Zhang, C.K.; Stive, M.J.F. Exploratory morphodynamic hindcast of the evolution of the abandoned Yellow River delta, 1578–1855 CE. *Mar. Geol.* **2017**, *383*, 99–119. [CrossRef]
54. Su, M.; Yao, P.; Wang, Z.B.; Zhang, C.K.; Stive, M.J.F. Exploratory morphodynamic modeling of the evolution of the Jiangsu coast, China, since 1855: Contributions of old Yellow River-derived sediment. *Mar. Geol.* **2017**, *390*, 306–320. [CrossRef]
55. Xing, F.; Wang, Y.P.; Wang, H.V. Tidal hydrodynamics and fine-grained sediment transport on the radial sand ridge system in the southern Yellow Sea. *Mar. Geol.* **2012**, *291–294*, 192–210. [CrossRef]